Chandra, Y., Saavedra Flores, E. I., Scarpa, F., & Adhikari, S. (2016). Buckling of hybrid nanocomposites with embedded graphene and carbon nanotubes. *Physica E: Low-dimensional Systems and Nanostructures*, *83*, 434-441. https://doi.org/10.1016/j.physe.2016.01.021

Buckling of hybrid nanocomposites with embedded graphene and carbon nanotubes

Y. Chandra[a], E.I. Saavedra Flores[b], F. Scarpa[c], S. Adhikari[a,*]

[a] *Zienkiewicz Centre for Computational Engineering, Swansea University, Swansea SA1 8EN, UK*
[b] *Departamento de Ingeniería en Obras Civiles, Universidad de Santiago de Chile, Av. Ecuador 3659, Estación Central, Santiago, Chile*
[c] *Advanced Composites Centre for Innovation and Science, University of Bristol, Bristol BS8 1TR, UK*

Abstract

With the aid of atomistic multiscale modelling and analytical approaches, buckling strength has been determined for carbon nanofibres/epoxy composite systems. Various nanofibers configurations considered are single walled carbon nano tube (SWCNT) and single layer graphene sheet (SLGS) and SLGS/SWCNT hybrid systems. Computationally, both eigen value and non linear large deformation based methods have been employed to calculate the buckling strength. The non-linear computational model generated here takes into account of complex features such as debonding between polymer and filler (delamination under compression), nonlinearity in the polymer, strain based damage criteria for the matrix, contact between fillers and interlocking of distorted filler surfaces with polymer. The effect of bridging nanofibers with an interlinking compound on the buckling strength of nanocomposites has also been presented here. Computed enhancement in buckling strength of the polymer system due to nano reinforcement is found to be in the range of experimental and molecular dynamics based results available in open literature. The findings of this work indicate that carbon based nanofillers enhance the buckling strength of host polymers through various local failure mechanisms.

Keywords: Graphene sheets; carbon nano tubes (CNT); hybrid nano-composites; atomistic model; mechanical properties of graphene and CNT based composites;

1. Introduction

Over the last few years, the investigation of carbon nano-materials has brought substantial progress, particularly in relation to the understanding of their mechanical [8, 12, 19, 42, 44, 46, 48, 49, 51, 54, 62, 63] and electrical [15, 24–26, 31, 58, 64, 69] properties. These nano-structures

*Corresponding author. Tel: +44 (0)1792 602088, Fax: + 44 (0)1792 295676
Email address: S.Adhikari@swansea.ac.uk (S. Adhikari)

have several applications as nanofillers for the reinforcement of polymer-based composite materials [3, 14, 16, 28]. In order to manufacture these nano-composites, different production methods have been proposed. For instance, graphene sheets can be mechanically exfoliated from graphite, chemically modified and then embedded in a polymeric solution [52]. Another alternative consists of dispersing graphene sheets in an organic solution to be used as stable fillers in polymers [57]. Furthermore, CNT-reinforced polymer composites can be manufactured by casting them in a polymer solution [11]. CNTs can also be dispersed in a solvent by sonication techniques. Then, they are mixed in a polymer liquid followed by evaporation of the initial solvent [45].

Methods to determine instabilities in SWCNTs under axial compression can be traced back to mid 1990s. Yakobson et al. [60] employed a body potential based technique to study the buckled shapes of SWCNT under compressive loads. The earliest computational work on buckling of graphene was done in late 2000s. Wilber et al. [59] used both continuum and atomistic approaches to simulate buckling in pair of interconnected graphene sheets. The buckling of such nano structures has also been computed using nonlocal continuum mechanics [33–36]. A molecular dynamics based study [10] on multi walled carbon nano tubes (MWCNT) revealed that only the outer layers of thick MWCNT undergo deformation under buckling loads. Saavedra Flores et al. [40] used hyperelastiticy to describe post buckling behaviour of SWCNTs, using atomistic simulations. Zhang et al. [68] dispersed oxidized SWNTs in polycarbonate matrices and reported 51% rise in buckling strength of the resulting composite structure. The experimental buckling strength of an epoxy-graphene platelet composite system, exceeded that of analytical buckling strength in the work of Rafiee et al. [37]. The authors suggested that the enhancement in the load transfer between the filler and matrix is the responsible for such discrepancy. The molecular dynamics based simulations in a SLGS/polymer system, have revealed delamination of SLGS under applied buckling loads [13]. Vodenitcharova and Zhang [56] used Airys stress function based analytical approach to calculate buckled deflections under bending loads on a SWCNT-Titanium composite system and demonstrated a localised ovalisation of the SWCNT. In 1998, the buckling of a MWCNT-polymer film composite system was observed experimentally [29]. The authors reported a compressive strength that is two orders of magnitude higher than the strength of any conventional fibre at that time. Parashar and Mertiny [32] developed an RVE (representative volume element) that can simulate compressive buckling in SLGS-polymer composite system across multiple length scales. Li and Chou [23] presented a multiscale model to compute the compressive strength of SWCNT reinforced polymer RVE. To the authors' knowl-

edge no work exists in the literature that considers high fidelity numerical simulation of nano reinforced polymers involving hybridisation and inter-bridging of fibers.

In order to predict the mechanical behaviour of graphene sheets and carbon nanotubes, several computational techniques have been proposed in the literature [8, 40, 41, 44, 49–51, 54]. One of these approaches is the finite element method, a technique which has been used successfully in engineering during the last decades and that has recently been used in the analysis of carbon nanostructures by Scarpa et al [8, 46, 48, 49] and Pour et al [43, 44], among others. Scarpa et al [8, 9, 46, 48, 49] proposed a numerical model in which the interatomic C-C bonds are replaced by equivalent (deep shear Timoshenko) beams with stretching, bending, torsional and shear deformation properties. These properties are determined by means of an equivalence between structural and molecular mechanics. In order to determine the mechanical behaviour of each interatomic bond, force constants are introduced within a harmonic potential function. The geometric configurations and mechanical properties are represented as truss assemblies (Finite Elements), for which the total potential energy associated to the loading conditions is calculated. The final thickness and equilibrium lengths of the bonds correspond to the minimum potential energy configuration of the nanostructure.

SLGS/SWCNT-reinforced nano-composites are represented by stiff nanoinclusions embedded in a softer polymeric surrounding matrix. SLGSs/SWCNTs can be modelled by an array of hexagonally-oriented beam elements. These beams represent the SP^2 covalent bonds, while the nodes of the same elements represent carbon atoms. At the meso and nanoscale level, the polymer matrix can be assumed as a continuum. Thus the polymer matrix can be modelled by an arrangement of 3D solid tetrahedral finite elements. In physical reality the polymer matrix is connected to carbon atoms through weak van der Waals forces, when no functional groups exist. These van der Waals forces can be represented by LJ potential forces. LJ potential attractive and repulsive forces between the inclusion and the matrix can be modelled by spring elements. This approach has been used by Li et al. [22] and Shokrieh et al.[50] to describe the mechanical response of epoxy/SWCNT composites.

With the aid of this numerical approach, five different geometrical configurations of nano-composites involving one or two nano fillers in each one are studied in the present work. Namely SWCNT nano-composite (Fig. 1), SLGS nano-composite (Fig. 2), SWCNT-SWCNT nano-composite (Fig. 3), SLGS-SLGS nano-composite (Fig. 4) and SWCNT-SLGS nano-composite (refer Fig. 5). In the nano-composites involving two nano-fillers, a chemical interlinker consist-

ing of an Aliphatic diamine $(CH_2)_{10}N_2H_4$ has been introduced to investigate its effect on the buckling strength.

Critical buckling load of nano-fibre reinforced epoxy polymer system are calculated analytically and numerically. In the latter case, numerical eigen-value buckling and nonlinear buckling-collapse analyses are performed. The non linear buckling analysis takes into account detailed features such as damage and non linearity in the polymer and in the filler, debonding/delamination and contact/interlocking of fillers/polymer. Therefore this analysis will be referred to as high fidelity analysis (HFA). The effect of different filler configurations on the buckling strength is investigated. A finite element-based multiscale approach is presented to simulate the buckling behavior of SLGS/SWCNT-reinforced nano-composites. At the macroscale level, the polymer matrix is represented by 3D solid elements with three translational and three rotational degrees of freedom per node. The weak interatomic bonds between the matrix and the fibre are modelled by nonlinear springs with mechanical properties governed by the LJ potential. At the nanoscale level, we adopt the atomistic-FE approach to describe the mechanical behaviour of SLGSs and SWCNTs. Nonlinear geometric displacement regime is considered in our finite element analyses.

2. Multiscale model of the composite structure

As commented previously, SP^2 covalent bonds in SWCNTs and SLGSs are modelled by deep shear Timoshenko beams. In order to perform all of our computational simulations, we select the finite element commercial software ABAQUS^{TM} version 6.10 [1] and its B31 beam element to model the covalent bonds. This type of element has three translational and 3 rotational degrees of freedom with shear correction. Here, we model each C-C bond beam with a length of 0.142 nm (the equilibrium length of C-C SP^2) and equivalent diameter of 0.089 nm [49]. The properties of the beams are calculated from the force constants given below [49]:

$$\frac{k_r}{2}(\delta r)^2 = \frac{EA}{2L}(\delta r)^2 \tag{1}$$

$$\frac{k_\tau}{2}(\delta \varphi)^2 = \frac{GJ}{2L}(\delta \varphi)^2 \tag{2}$$

$$\frac{k_\theta}{2}(\delta \theta)^2 = \frac{EI}{2L}\frac{4+\Phi}{1+\Phi}(\delta \theta)^2 \tag{3}$$

In the above equations, k_r represents the stretching force constant and k_τ the out-of-plane torsional constant. The force constant k_θ represents combined in-plane rotation (i.e., bending and torsion), which is consistent with the harmonic potential approach [49]. The term Φ is the

shear correction factor, which becomes significant if the aspect ratio of the beam is lower than 10 [53]. The above constants can be obtained from the Morse or Amber potential models [49]. According to the Morse model, the values of the force constants are $k_r = 8.74 \times 10^{-7}\mathrm{N\,mm^{-1}}$, $k_\theta = 9.00 \times 10^{-10}\mathrm{N\,nm\,rad^{-2}}$ and $k_\tau = 2.78 \times 10^{-10}\mathrm{N\,nm^{-1}\,rad^{-2}}$. For those readers interested in further information on this methodology, we refer, for instance, to [46, 47, 49]. With the above values of force constants, it is straightforward to obtain Table 2 with the equivalent properties of the C-C bond beams for the modelling of SLGSs and SWCNTs.

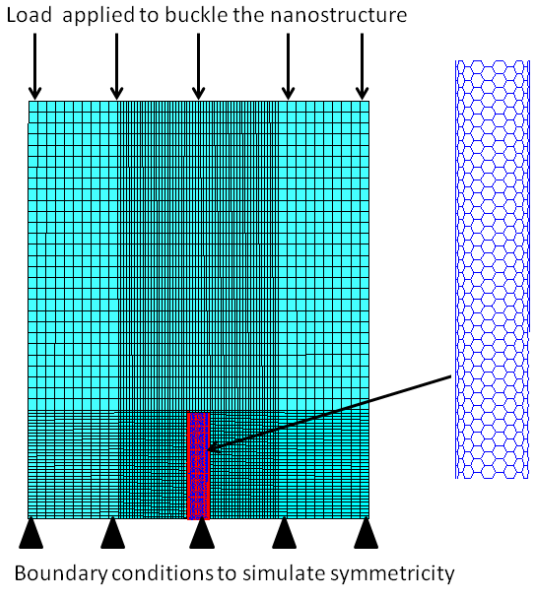

Fig. 1: SWCNT nanocomposite with boundary conditions. Note: The nano fillers (SWCNT lattice structures) are connected to surrounding polymer through vdW spring elements.

In the current work the non linearity and damage of covalent bonds in SLGS/SWCNT plays a vital role in deciding the buckling strength of host polymer. An equivalent stress-strain curve for SP^2 C-C covalent has been implemented under both comprehension and tension. This stress-strain curve is based on the modified Morse potential bonds derived by other authors [5, 6, 17, 30, 55]. The points on the curve are shown in Fig. 7. The single C-C bond shows a non linear regime under both tension and compression at larger strains [5]. Under buckling loads on nanocomposites in the current work, the C-C bonds are subjected to larger strains of both tension and compressive nature. Based on the inflection point in C-C bonds determined by Tserpes et al. [55], a damage criterion of 19% strain has been specified for the beam elements.

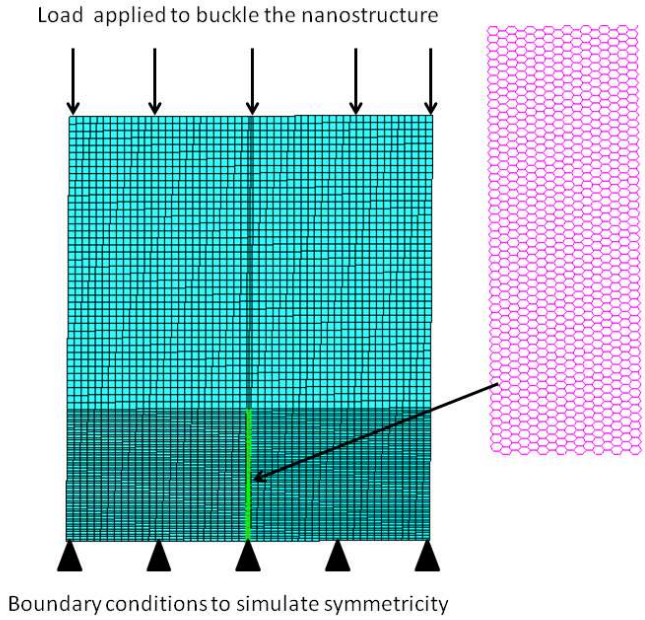

Fig. 2: SLGS nanocomposite with boundary conditions. Note: The nano fillers (SLGS lattice structures) are connected to surrounding polymer through vdW spring elements.

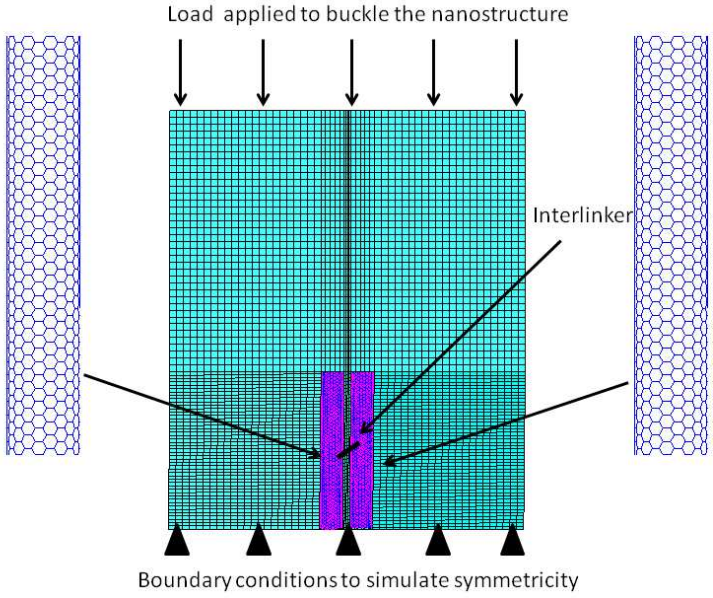

Fig. 3: SWCNT-SWCNT nanocomposite with boundary conditions. Note: The nano fillers (SWCNT lattice structures) are connected to surrounding polymer through vdW spring elements.

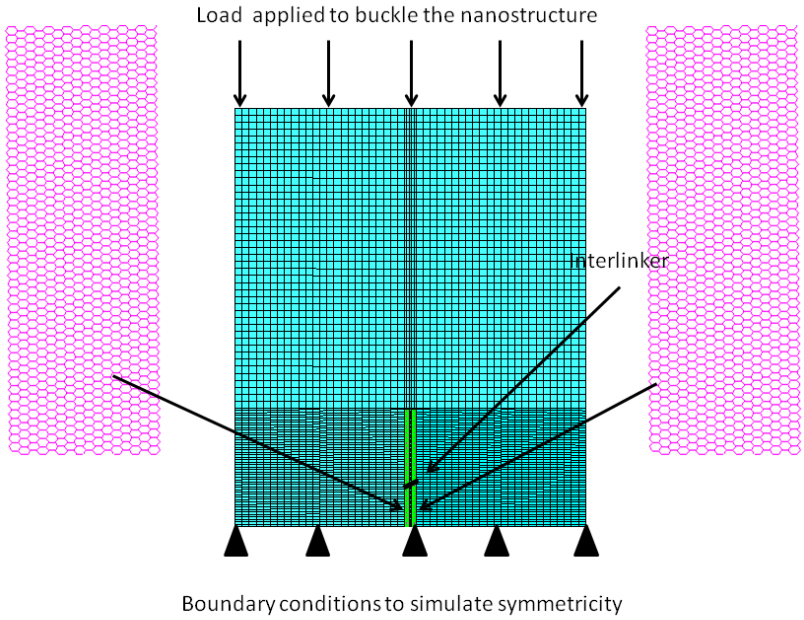

Fig. 4: SLGS-SLGS nanocomposite with boundary conditions. Note: The nano fillers (SWCNT SLGS lattice structures) are connected to surrounding polymer through vdW spring elements.

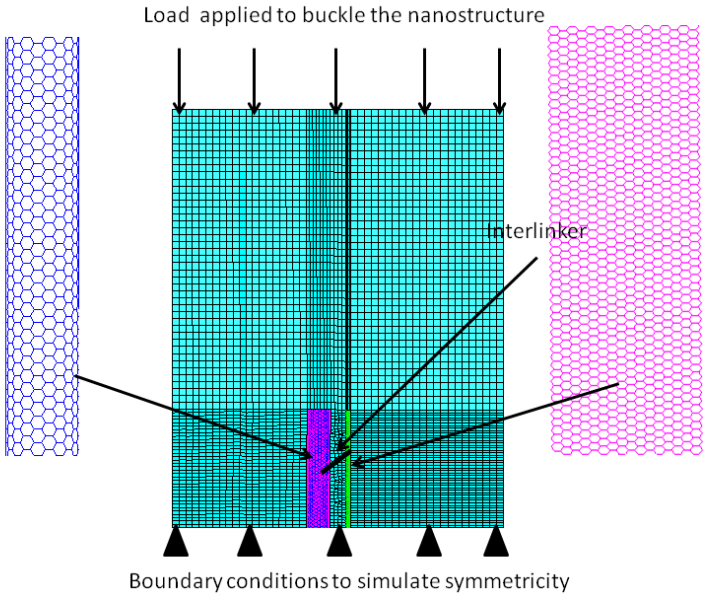

Fig. 5: SLGS-SWCNT nanocomposite with boundary conditions. Note: The nano fillers (SWCNT and SLGS lattice structures) are connected to surrounding polymer through vdW spring elements.

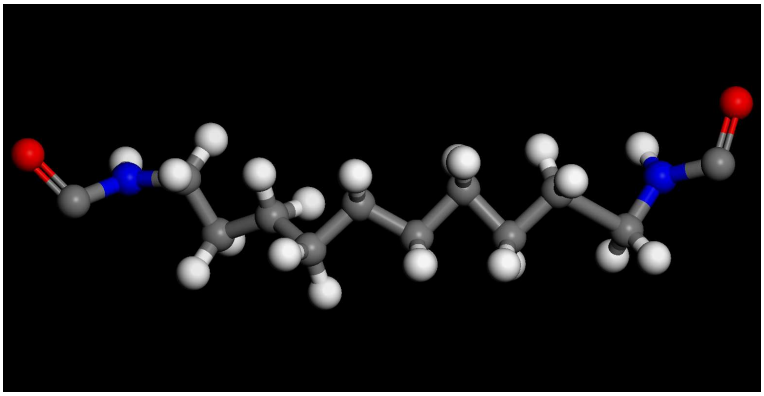

Fig. 6: Aliphatic diamine $(CH_2)_{10}N_2H_4$ inter-linker used to bridge fillers in nano-composites.

Table 1: Element properties for the beam elements used to represent CC bonds. In the table, d is diameter, l is length, A is cross sectional area, E is Young's modulus, ν is Poisson's ratio and ϕ is the shear correction factor [2].

Property	Value
d	0.089 nm
l	0.142 nm
A	1.01 nm^2
E	19.5 TPa
ν	0.23
ϕ	0.37

This means if the strain in beam elements representing covalent bonds goes beyond 19%, then their stiffness will be reduced to zero.

Similar to that of C-C bonds, the mechanical properties of other bonds in the inter-linker can also be obtained by universal force field (UFF) [2, 39]. These mechanical properties are presented in Table 3.

Graphene sheets are linked to the polymer matrix by means of van der Waals interaction forces, which can be represented mathematically as:

$$F_{ij} = \frac{\partial V_{ij}}{\partial r} \tag{4}$$

where, r is the atomic displacement along **ij** (fibre-matrix length). As per Girifalco et al [18],

Table 2: Thicknesses, lengths and Young's moduli for bonds in inter-linkers [2].

Bond types	Bond length (A^o)	Bond thickness (A^o)	Young's Modulus [TPa]
CH	1.08	1.01	6
CN	1.39	0.79	23.5
HN	1.01	0.8	16

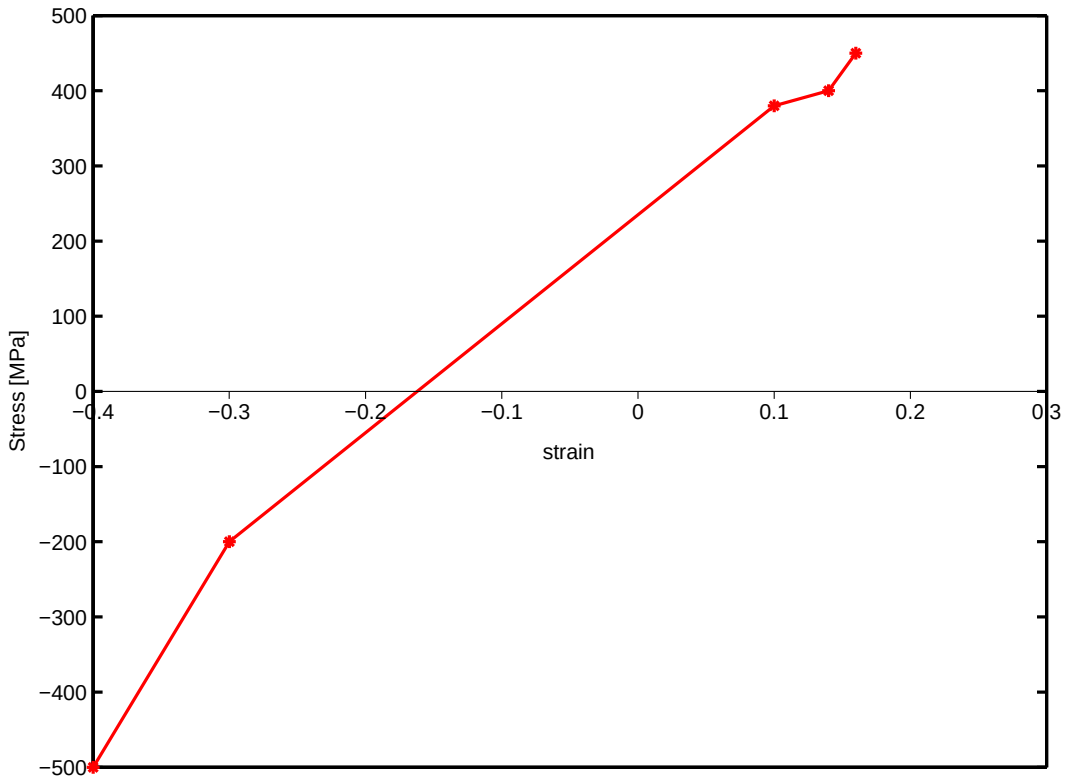

Fig. 7: Points of the stress-strain curve for C-C bonds [5, 6]

the force between the atoms (ij) can also be represented by

$$F_{ij} = -12\,\epsilon \left[\left(\frac{r_{min}}{y} \right)^{13} - \left(\frac{r_{min}}{y} \right)^{7} \right] \tag{5}$$

where, $y = r_{min} + \delta r$, δr is the atomic displacement along the length **ij**. The r_{min} (in Å) is given by $2^{\frac{1}{6}}\,\sigma$, where $\sigma = (A/B)^{1/6}$. Here, B and A are attractive and repulsive constants associated to the corresponding boundary conditions, with values of 3.4×10^{-4} $eV\times$ Å^{12} and 5×10^{-7} $eV\times$ Å^{6}, respectively [4, 18, 50]. The constant ϵ is given by the expression $B^2/(4A)$. In our multiscale models we use the nonlinear spring element SPRINGA to simulate this interaction in ABAQUS^{TM}, with an equivalent force-deflection curve given by Eq. 5. We note that this approach has been used recently to model the attractive and repulsive forces between adjacent layers of multi-layer graphene sheets [8].

3D solid elements with six degrees of freedom per node are selected to model the matrix. The type of element used in ABAQUS^{TM} is C3D4. In order to make optimum use of computational time, the mesh density of the matrix is set to ensure that, there lies a coincident node in the 3D matrix on top each carbon atom in the filler. Isotropic material properties are assumed to represent the mechanical behavior of an epoxy matrix, with Young's modulus of 2.0 GPa

and Poisson's ratio of 0.3 [61]. A curve based on experimental work by Littell et al [27], is adopted to capture the material tensile and compressive nonlinearity present in the matrix, with a corresponding stress-strain curve given by Fig. 8. A strain-based damage criterion based on the approximated maximum elongation in the formerly mentioned curve, is assigned to the matrix, such that the stiffness of those finite elements strained over 20 % is zero.

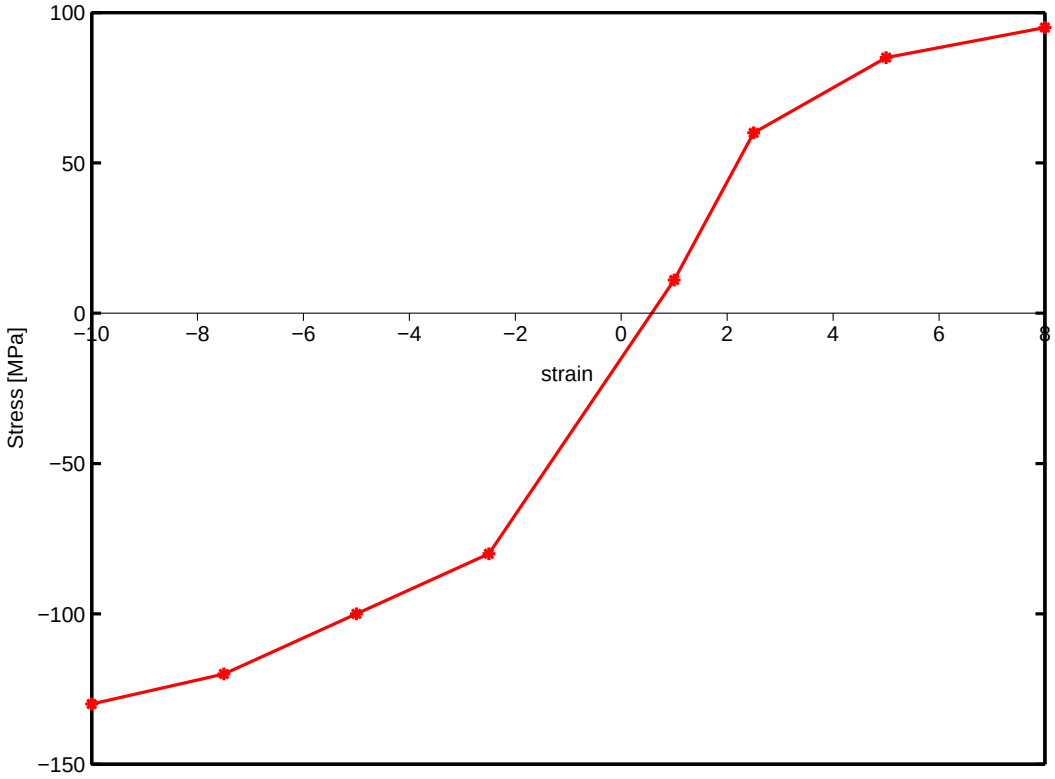

Fig. 8: Points of the stress-strain curve for C-C bonds [5, 6]

The SWCNT modelled is armchair type (16,225) and of length 48 nm. The SLGS modelled is armchair type (16,225) and of length 48 nm. These dimensions of SLGS and SWCNT ensure that both fillers have same surface area. As SLGS offers a 2D surface, the contact interface with polymer molecules, occurs at both surfaces (top and bottom of SLGS sheets). For the epoxy matrix around the filler, appropriate dimensions have been chosen to obtain desired weight fractions (0.05% and 0.1%) and slenderness ratio. The dimension of the overall composite system is 86x86x708 leading to a rectangular beam. The nonlinear force-deflection curves for LJ-potentials, both in tension and compression are derived from Equation 5. A node to element contact definition has been assigned between the nodes of the filler, inter-linkers and the surface of 3D elements in polymer matrix. A Eigen value buckling analysis and a nonlinear Newton-Raphson solver with switch on large deformation effects has been performed on the

nanocomposites [1]. The simulation has been run until the filler structure becomes unstable due to fracture strain in C-C bonds.

We note that during our simulations, the interface bonds (spring elements) between the filler and the matrix are deactivated if the deflection developed is greater than the cut-off distance of 0.85 nm [50]. Similarly, new interatomic bonds are regenerated if a displaced carbon atom comes in contact with another atom of the matrix. The nodal displacements in the nonlinear spring elements (interface bonds) are measured at each load step. If the nodal displacement is found to exceed the cut-off distance, the analysis is stopped and restarted with an updated position of the nodes belonging to the spring elements. This process analysis stop and restart is referred to as debonding and rebonding mechanism in the present work. This computational routine is implemented in Python programming language within ABAQUS^{TM}. We remark here that one of the main motivations to choose ABAQUS^{TM} for our analyses is its capability to incorporate damage laws in composites along with the use of user-defined subroutines written in Python. In the context of finite element analysis, the numerical buckling mode is calculated by [1]:

$$(K_0 + \lambda_i K_\delta)v_i = 0 \tag{6}$$

In the above equation, K_0 is the stiffness matrix at base state, K_δ is differential stiffness matrix, λ_i is the vector of Eigen values v_i is the vector of buckled mode shapes. In the case of HFA simulations, the iterative equations to be evaluated are:

$$K_i + c_{i+1} = F_i \tag{7}$$

$$K_i = \frac{\partial F}{\partial u} u_i \tag{8}$$

$$F_i = F(u_i) \tag{9}$$

$$u_{i+1} = c_{i+1} + u_i \tag{10}$$

Where i indicates the iteration number, K_i is the jacobian matrix, c_{i+1} is difference between approximate and exact solutions of the deflection u, u_i and u_{i+1} are the solutions for deflection u at ith and i+1th iterations respectively, F_i is the vector of force components and is also a function of u_i. The above equations are solved iteratively until the term c_{i+1} becomes negligible. Once the convergence is obtained, the secondary variables such as strains and stresses are computed using

the vector u_i. For comprehensive understanding of the above mentioned numerical procedures, the readers are referred to ABAQUS^{TM} documentation [1].

The dimensions chosen for nano composite structures makes the structure slender. Analytically, the critical load required to buckle such slender structure can be calculated by Euler's formula. The boundary conditions considered here are simply supported at one end (simulating symmetry) and load applied at the other end of the column (Fig. 1). The classical Euler's formula of buckling under such conditions takes the form of [7, 21]:

$$P_{cr} = \frac{(\pi^2)E_c I}{L^2} \tag{11}$$

Where P_{Cr} is the critical buckling load, I is the moment of inertia, L is the length of the column and E_c is the Youngs modulus of the composite system derived from rule of mixtures [20] shown below.

$$E_c = V_f\ E_f + V_m\ E_m \tag{12}$$

In the above relations, E_f is the elastic modulus of the fibre, E_m is the elastic modulus of the matrix, V_f is the volume fraction of the fibre, V_m is the volume fraction of the matrix.

3. Results and discussions

The buckling strength computed by Eq. 11 has been compared with the numerical solutions shown in Table 3. In this analysis two realistic weight fractions are considered. These are 0.05 % and 0.1 % [38]. The Eq. 11 predicted 7% and 24% enhancement in buckling strength due to filler weight fractions 0.05 % and 0.1 %, respectively. However the enhancements predicted by the numerical models are found to be higher than those predicted analytically, for a given volume fraction. The interfacial mechanisms of the computational atomistic simulations are responsible for such discrepancies. A similar trend has been observed in some experimental works [37, 68]. The analytical critical buckling load calculated for the neat matrix (P_m) is very close to the numerical prediction. As per the Eigenvalue analysis, the configuration of fillers associated with the highest buckling resistance is the SLGS-SLGS type. In regards to HFA solutions, the configuration SWCNT-SWCNT offers the highest buckling resistance. In HFA simulations, geometrical distortions in SWCNTs (ovalisation) lead to interlocking of these fillers resulting in increased buckling resistance. Such geometrical distortions are observed only in HFA simulations, but not in Eigenvalue analysis. This is due to the fact that HFA includes

Table 3: Buckling strength computed by analytical (Eq. 11), Eigen value and non linear analysis. P_c is critical buckling load of the nanocomposite. P_m is critical buckling load of neat matrix of same dimensions as that of corresponding nanocomposite.

Analysis type	Filler type	Wt-frctn(%)	P_c(N)	P_m(N)	Enhancement(%)
Analytical	Any	0.05	38.5	35.9	7
Analytical	Any	0.1	44.8	35.9	24
Eigen value	SLGS	0.05	54.3	42.8	26
Eigen value	SWCNT	0.05	51.8	42.8	21
Eigen value	SWCNT-SWCNT	0.1	54.6	42.8	27
Eigen value	SLGS-SLGS	0.1	64.4	42.8	50
Eigen value	SWCNT-SLGS	0.1	59.7	42.8	39
Eigen value	SWCNT-interlinker-SWCNT	0.1	55.4	42.8	29
Eigen value	SLGS-interlinker-SLGS	0.1	65.3	42.8	52
Eigen value	SWCNT-interlinker-SLGS	0.1	60.6	42.8	41
HFA model	SLGS	0.05	60.6	40.1	51
HFA model	SWCNT	0.05	54.6	40.1	36
HFA model	SWCNT-SWCNT	0.1	67.1	40.1	68
HFA model	SLGS-SLGS	0.1	62.4	40.1	55
HFA model	SWCNT-SLGS	0.1	63.24	40.1	57
HFA model	SWCNT-interlinker-SWCNT	0.1	67.8	40.1	69
HFA model	SLGS-interlinker-SLGS	0.1	64.8	40.1	57
HFA model	SWCNT-interlinker-SLGS	0.1	65.2	40.1	59

Table 4: Comparison of enhancement of buckling strength due to nanoinclusion by present work against previous literature

Study	Analysis type	Filler type	Wt-frctn(%)	Maximum Enhancement observed(%)
Present	Analytical	Any	0.05	7
Present	Analytical	Any	0.1	24
Present	Eigen value	3 configurations studied	0.05	26
Present	Eigen value	3 configurations studied	0.1	52
Present	HFA model	3 configurations studied	0.05	51
Present	HFA model	3 configurations studied	0.1	69
Rafiee et al. [37]	Experimental	Graphene platelets	0.1	52
Zhang et al. [68]	Experimental	SWCNT	1	51
Parashar and Mertiny [32]	Numerical	SLGS	6	26

large deformation effects. In general, it can also be observed that the increase of the filler weight fraction from 0.05% to 0.1% enhances the buckling resistance, up to 69% (as per HFA SWCNT-interlinker-SWCNT model). Weight fractions higher than those studied here can be difficult to obtain due to dispersion issues [52]. Table 3 also shows that the introduction of chemical inter-linkers between fillers increases further the buckling strength. This is in agreement with previous works [65–67] that indicate alleviation of the structure performance due to chemical linkers between fillers. In general, the increase of the buckling resistance due to the inclusion of nano-reinforcements is comparable with those values reported by other authors [32, 37, 68] and shown in Table 4.

In HFA methodology, one end of the structure has been supported and an increasing load has been applied at the other end (refer to Fig. 1). This load has been increased progressively in small steps until the (slender) structure becomes unstable. During this incremental analysis, the sudden decrease in load required to cause deflections in the structure indicates the onset of collapse or buckling. The magnitude of stress (in Mpa) at this step is the critical buckling load or compressive failure stress. This process has been shown in the Fig. 10. In the initial segment of the curve, the load required to cause the deflection increases in smaller magnitudes. This shows a lower value of slope for the curve during the initial increments. This is due to the fact that the applied load is mainly taken by the polymer (refer Fig. 1). This slope is found to be the same for all the curves (and the volume of the polymer is approximately the same for all the simulated nanocomposites). At a strain of about 0.4%, an increase in the slope is observed. This indicates that the load is transferred to filler from the surrounding polymer. Beyond the initial portion of the curve, the nanocomposite with weight fraction 0.1% requires a higher load to deform the structure, when compared to the nanocomposites with 0.05 %. After the initial segment of the curve, the slope of the nanocomposite with SLGS-SLGS remains constant. But for those nanocomposites involving SWCNT-SWCNT and SLGS-SWCNT, the slope changes at a strain level 0.15 level close to 4 nm. This is due to the ovalisation of SWCNT tubes, which causes fillers to rub each other and consequently enhance the buckling resistance. However, this effect might not lead to such strength enhancement if the distance between the fillers is greater than the one adopted in our simulations. The ovalisation of SWCNTs will also lead to an interlocking between fillers and the surrounding polymer. Fig. 10 shows that the nanocomposite with SWCNT-interlinker-SWCNT filler offers the highest resistance. The magnitude of the compressive strength in this particular nanocomposite is found to be 148

MPa, whereas the compressive strength of the nanocomposite with SWCNT-SWCNT filler is found to be 145 MPa. That is, the introduction of additional chemical interlinkers among fillers can enhance further the compressive strength.

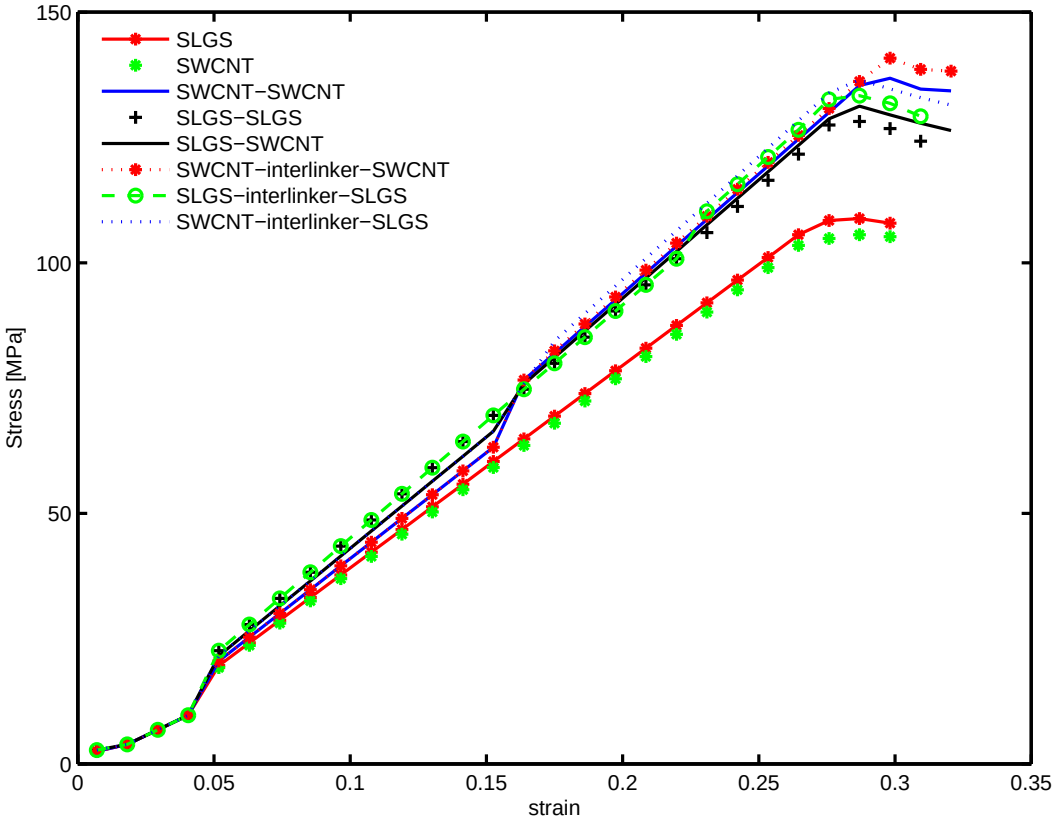

Fig. 9: Prediction of buckling in nanocomposite using HFA methodology.

4. Conclusion

Buckling strength has been calculated for SLGS, SWCNT and SLGS-SWCNT hybrid nanocomposites by a multiscale computational modelling framework. Here, two numerical approaches have been adopted: an eigenvalue analysis and a non linear high fidelity analysis (HFA). The proposed multiscale models have taken into account the complex failure mechanisms found in nanocomposite structures. These models have been able to reproduce buckling mode shapes and capture local structural behaviour of nanocomposites at failure. In both numerical analyses, the predicted critical buckling load has shown strong dependency on the filler types and their configurations. The results of our two numerical approaches have been compared with the analytical solutions obtained from continuum theory. Lower buckling loads have been determined by the analytical method. These low values can be attributed to the detailed modelling of the interface

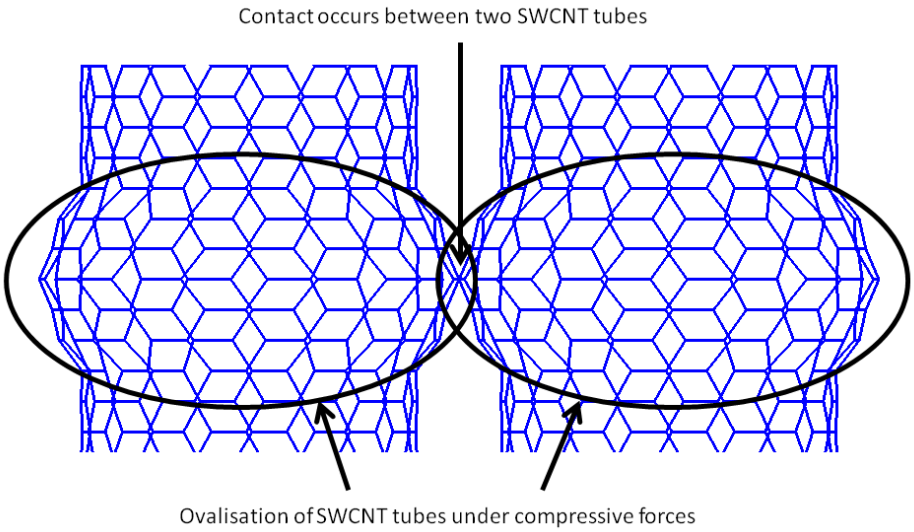

Fig. 10: Increase in buckling resistance in SWCNT-SWCNT nanocmposite due to ovalisation and resulting contact.

between fillers and the matrix. The eigenvalue buckling analysis has indicated an increase up to 50% in the buckling strength of the composite system due to the nano reinforcement of two SLGSs. The HFA has shown an increase of 69 % due to the nano reinforcement of two SWCNTs. Such differences between the two numerical strategies indicate the necessity of high fidelity numerical models in nanomechanics. The interfacial characteristics such as contact surface area between the filler and the matrix, contact among fillers and the strength of bonding between the filler and the matrix play a vital role to predict accurately the buckling response. Furthermore, the introduction of a chemical interlinking compound between two nanofillers enhances the buckling strength of the nanocomposite.

Thus, the complex and intricate micro-mechanisms of interaction found among fillers, interlinkers and the matrix of nanocomposites have shown great influence on their buckling response. These features have been captured successfully by the present multiscale modelling approach, paving the way for further investigation on the mechanics and physics of nanocomposite materials.

Acknowledgements

FS thanks the support of the FP7-NMP-2010-LA-2010-246067 M-RECT project for the logistics support.

References

[1] Abaqus: Documentation and User Manual (2012). Version 6.12. *Simulia, Dassault Systèmes*.

[2] Adhikari, S., Saavedra Flores, E. I., Scarpa, F., Chowdhury, R., and Friswell, M. I. (2014). A hybrid atomistic approach for the mechanics of deoxyribonucleic acid molecules. *Journal of Nanotechnology in Engineering and Medicine*, 4(4):041003–041003.

[3] Andrews, R. and Weisenberger, M. (2004). Carbon nanotube polymer composites. *Current Opinion in Solid State and Materials Science*, 8(1):31–37.

[4] Battezzati, L., Pisani, C., and Ricca, F. (1975). Equilibrium conformation and surface motion of hydrocarbon molecules physisorbed on graphit. *Journal of the Chemical Society, Faraday Transactions 2: Molecular and Chemical Physics*, 71:1629–1639.

[5] Baykasoglu, C. and Mugan, A. (2012a). Coupled molecular/continuum mechanical modeling of graphene sheets. *Physica E: Low-dimensional Systems and Nanostructures*, 45:151–161.

[6] Baykasoglu, C. and Mugan, A. (2012b). Nonlinear fracture analysis of single-layer graphene sheets. *Engineering Fracture Mechanics*, 96:241–250.

[7] Budynas, R. G. and Nisbett, J. (2011). Shigley's mechanical engineering design.

[8] Chandra, Y., Chowdhury, R., Scarpa, F., and Adhikari, S. (2011). Vibrational characteristics of bilayer graphene sheets. *Thin Solid Films*, 519(18):6026–6032.

[9] Chandra, Y., Scarpa, F., Chowdhury, R., Adhikari, S., and Sienz, J. (2013). Multiscale hybrid atomistic-fe approach for the nonlinear tensile behaviour of graphene nanocomposites. *Composites Part A: Applied Science and Manufacturing*, 46:147–153.

[10] Chang, T. and Hou, J. (2006). Molecular dynamics simulations on buckling of multiwalled carbon nanotubes under bending. *Journal of applied physics*, 100(11):114327.

[11] Chen, W. and Tao, X. (2006). Production and characterization of polymer nanocomposite with aligned single wall carbon nanotubes. *Applied Surface Science*, 252(10):3547–3552.

[12] Chowdhury, R., Adhikari, S., Scarpa, F., and Friswell, M. I. (2011). Transverse vibration of single-layer graphene sheets. *Journal of Physics D: Applied Physics*, 44(20):205401.

[13] Cranford, S. W. (2013). Buckling induced delamination of graphene composites through hybrid molecular modeling. *Applied Physics Letters*, 102(3):031902.

[14] DAloia, A., Marra, F., Tamburrano, A., De Bellis, G., and Sarto, M. (2014). Electromagnetic absorbing properties of graphene–polymer composite shields. *Carbon*, 73:175–184.

[15] Dimitrakopoulos, C., Lin, Y.-M., Grill, A., Farmer, D. B., Freitag, M., Sun, Y., Han, S.-J., Chen, Z., Jenkins, K. A., Zhu, Y., et al. (2010). Wafer-scale epitaxial graphene growth on the si-face of hexagonal sic (0001) for high frequency transistors. *Journal of Vacuum Science & Technology B*, 28(5):985–992.

[16] Du, J. and Cheng, H.-M. (2012). The fabrication, properties, and uses of graphene/polymer composites. *Macromolecular Chemistry and Physics*, 213(10-11):1060–1077.

[17] Georgantzinos, S., Giannopoulos, G., and Anifantis, N. (2009). Investigation of stress–strain behavior of single walled carbon nanotube/rubber composites by a multi-scale finite element method. *Theoretical and Applied Fracture Mechanics*, 52(3):158–164.

[18] Girifalco, L., Hodak, M., and Lee, R. S. (2000). Carbon nanotubes, buckyballs, ropes, and a universal graphitic potential. *Physical Review B*, 62(19):13104.

[19] Gupta, S. and Batra, R. (2010). Elastic properties and frequencies of free vibrations of single-layer graphene sheets. *Journal of Computational and Theoretical Nanoscience*, 7(10):2151–2164.

[20] Hull, D. and Clyne, T. (1996). *An introduction to composite materials*. Cambridge university press.

[21] J. Singer, J. A. and Weller, T. (1998). Buckling experiments: Experiments in thin-walled structures: Basic concepts, columns, beams and plates. 1.

[22] Li, C. and Chou, T.-W. (2003). A structural mechanics approach for the analysis of carbon nanotubes. *International Journal of Solids and Structures*, 40(10):2487–2499.

[23] Li, C. and Chou, T.-W. (2006). Multiscale modeling of compressive behavior of carbon nanotube/polymer composites. *Composites science and technology*, 66(14):2409–2414.

[24] Liang, J., Wang, Y., Huang, Y., Ma, Y., Liu, Z., Cai, J., Zhang, C., Gao, H., and Chen, Y. (2009a). Electromagnetic interference shielding of graphene/epoxy composites. *Carbon*, 47(3):922–925.

[25] Liang, J., Xu, Y., Huang, Y., Zhang, L., Wang, Y., Ma, Y., Li, F., Guo, T., and Chen, Y. (2009b). Infrared-triggered actuators from graphene-based nanocomposites. *The Journal of Physical Chemistry C*, 113(22):9921–9927.

[26] Lin, Y.-M., Dimitrakopoulos, C., Jenkins, K. A., Farmer, D. B., Chiu, H.-Y., Grill, A., and Avouris, P. (2010). 100-ghz transistors from wafer-scale epitaxial graphene. *Science*, 327(5966):662–662.

[27] Littell, J. D., Ruggeri, C. R., Goldberg, R. K., Roberts, G. D., Arnold, W. A., and Binienda, W. K. (2008). Measurement of epoxy resin tension, compression, and shear stress–strain curves over a wide range of strain rates using small test specimens. *Journal of Aerospace Engineering*, 21(3):162–173.

[28] Liu, Y. and Kumar, S. (2014). Polymer/carbon nanotube nano composite fibers. *ACS Applied Materials & Interfaces*, 6(9):6069–6087. PMID: 24520802.

[29] Lourie, O., Cox, D., and Wagner, H. (1998). Buckling and collapse of embedded carbon nanotubes. *Physical Review Letters*, 81(8):1638.

[30] Mohammadpour, E. and Awang, M. (2012). Nonlinear finite-element modeling of graphene and single-and multi-walled carbon nanotubes under axial tension. *Applied Physics A*, 106(3):581–588.

[31] Novoselov, K. S., Geim, A. K., Morozov, S., Jiang, D., Zhang, Y., Dubonos, S., Grigorieva, I., and Firsov, A. (2004). Electric field effect in atomically thin carbon films. *science*, 306(5696):666–669.

[32] Parashar, A. and Mertiny, P. (2012). Representative volume element to estimate buckling behavior of graphene/polymer nanocomposite. *Nanoscale research letters*, 7(1):1–6.

[33] Pradhan, S. (2009). Buckling of single layer graphene sheet based on nonlocal elasticity and higher order shear deformation theory. *Physics Letters A*, 373(45):4182–4188.

[34] Pradhan, S. (2012). Buckling analysis and small scale effect of biaxially compressed graphene sheets using non-local elasticity theory. *Sadhana*, 37(4):461–480.

[35] Pradhan, S. and Murmu, T. (2009). Small scale effect on the buckling of single-layered graphene sheets under biaxial compression via nonlocal continuum mechanics. *Computational Materials Science*, 47(1):268–274.

[36] Pradhan, S. and Phadikar, J. (2010). Scale effect and buckling analysis of multilayered graphene sheets based on nonlocal continuum mechanics. *Journal of Computational and Theoretical Nanoscience*, 7(10):1948–1954.

[37] Rafiee, M., Rafiee, J., Yu, Z.-Z., and Koratkar, N. (2009a). Buckling resistant graphene nanocomposites. *Applied Physics Letters*, 95(22):223103.

[38] Rafiee, M. A., Rafiee, J., Wang, Z., Song, H., Yu, Z.-Z., and Koratkar, N. (2009b). Enhanced mechanical properties of nanocomposites at low graphene content. *ACS nano*, 3(12):3884–3890.

[39] Rappé, A. K., Casewit, C. J., Colwell, K., Goddard Iii, W., and Skiff, W. (1992). Uff, a full periodic table force field for molecular mechanics and molecular dynamics simulations. *Journal of the American Chemical Society*, 114(25):10024–10035.

[40] Saavedra Flores, E. I., Adhikari, S., Friswell, M. I., and Scarpa, F. (2011a). Hyperelastic axial buckling of single wall carbon nanotubes. *Physica E: Low-dimensional Systems and Nanostructures*, 44(2):525–529.

[41] Saavedra Flores, E. I., Adhikari, S., Friswell, M. I., and Scarpa, F. (2011b). Hyperelastic finite element model for single wall carbon nanotubes in tension. *Computational Materials Science*, 50(3):1083–1087.

[42] Sadeghi, M. and Naghdabadi, R. (2010). Nonlinear vibrational analysis of single-layer graphene sheets. *Nanotechnology*, 21(10):105705.

[43] Sakhaee-Pour, A. (2009). Elastic buckling of single-layered graphene sheet. *Computational Materials Science*, 45(2):266–270.

[44] Sakhaee-Pour, A., Ahmadian, M., and Naghdabadi, R. (2008). Vibrational analysis of single-layered graphene sheets. *Nanotechnology*, 19(8):085702.

[45] Satyanarayana, N., Rajan, K. S., Sinha, S. K., and Shen, L. (2007). Carbon nanotube reinforced polyimide thin-film for high wear durability. *Tribology letters*, 27(2):181–188.

[46] Scarpa, F. and Adhikari, S. (2008). A mechanical equivalence for poisson's ratio and thickness of c–c bonds in single wall carbon nanotubes. *Journal of Physics D: Applied Physics*, 41(8):085306.

[47] Scarpa, F., Adhikari, S., and Chowdhury, R. (2010a). The transverse elasticity of bilayer graphene. *Physics Letters A*, 374(19–20):2053 – 2057.

[48] Scarpa, F., Adhikari, S., Gil, A., and Remillat, C. (2010b). The bending of single layer graphene sheets: the lattice versus continuum approach. *Nanotechnology*, 21(12):125702.

[49] Scarpa, F., Adhikari, S., and Phani, A. S. (2009). Effective elastic mechanical properties of single layer graphene sheets. *Nanotechnology*, 20(6):065709.

[50] Shokrieh, M. M. and Rafiee, R. (2010a). On the tensile behavior of an embedded carbon nanotube in polymer matrix with non-bonded interphase region. *Composite Structures*, 92(3):647 – 652.

[51] Shokrieh, M. M. and Rafiee, R. (2010b). Prediction of youngs modulus of graphene sheets and carbon nanotubes using nanoscale continuum mechanics approach. *Materials & Design*, 31(2):790–795.

[52] Stankovich, S., Dikin, D. A., Dommett, G. H., Kohlhaas, K. M., Zimney, E. J., Stach, E. A., Piner, R. D., Nguyen, S. T., and Ruoff, R. S. (2006). Graphene-based composite materials. *Nature*, 442(7100):282–286.

[53] Timoshenko, S., Woinowsky-Krieger, S., and Woinowsky-Krieger, S. (1959). *Theory of plates and shells*, volume 2. McGraw-hill New York.

[54] Tserpes, K. and Papanikos, P. (2005). Finite element modeling of single-walled carbon nanotubes. *Composites Part B: Engineering*, 36(5):468–477.

[55] Tserpes, K., Papanikos, P., and Tsirkas, S. (2006). A progressive fracture model for carbon nanotubes. *Composites Part B: Engineering*, 37(7):662–669.

[56] Vodenitcharova, T. and Zhang, L. (2006). Bending and local buckling of a nanocomposite beam reinforced by a single-walled carbon nanotube. *International journal of solids and structures*, 43(10):3006–3024.

[57] Wajid, A. S., Das, S., Irin, F., Ahmed, H., Shelburne, J. L., Parviz, D., Fullerton, R. J., Jankowski, A. F., Hedden, R. C., and Green, M. J. (2012). Polymer-stabilized graphene dispersions at high concentrations in organic solvents for composite production. *Carbon*, 50(2):526–534.

[58] Wang, T., Chen, G., Wu, C., and Wu, D. (2007). Study on the graphite nanosheets/resin shielding coatings. *Progress in organic coatings*, 59(2):101–105.

[59] Wilber, J. P., Clemons, C. B., Young, G. W., Buldum, A., and Quinn, D. D. (2007). Continuum and atomistic modeling of interacting graphene layers. *Physical Review B*, 75(4):045418.

[60] Yakobson, B. I., Brabec, C., and Bernholc, J. (1996). Nanomechanics of carbon tubes: instabilities beyond linear response. *Physical review letters*, 76(14):2511.

[61] Yarrington, P., Zhang, J., Collier, C., and Bednarcyk, B. A. (2005). Failure analysis of adhesively bonded composite joints. In *46 th AIAA/ASME/ASCE/AHS/ASC Structures, Structural Dynamics & Materials Conference*.

[62] Yu, M.-F., Files, B. S., Arepalli, S., and Ruoff, R. S. (2000a). Tensile loading of ropes of single wall carbon nanotubes and their mechanical properties. *Physical review letters*, 84(24):5552.

[63] Yu, M.-F., Lourie, O., Dyer, M. J., Moloni, K., Kelly, T. F., and Ruoff, R. S. (2000b). Strength and breaking mechanism of multiwalled carbon nanotubes under tensile load. *Science*, 287(5453):637–640.

[64] Zhang, H.-B., Zheng, W.-G., Yan, Q., Yang, Y., Wang, J.-W., Lu, Z.-H., Ji, G.-Y., and Yu, Z.-Z. (2010). Electrically conductive polyethylene terephthalate/graphene nanocomposites prepared by melt compounding. *Polymer*, 51(5):1191–1196.

[65] Zhang, J. and Jiang, D. (2011). Interconnected multi-walled carbon nanotubes reinforced polymer-matrix composites. *Composites Science and Technology*, 71(4):466 – 470.

[66] Zhang, J., Jiang, D., and Peng, H.-X. (2013a). Two-stage mechanical percolation in the epoxy resin intercalated buckypaper with high mechanical performance. *RSC Advances*, 3(35):15290–15297.

[67] Zhang, J., Jiang, D., Scarpa, F., and Peng, H.-X. (2013b). Enhancement of pullout energy in a single-walled carbon nanotube-polyethylene composite system via auxetic effect. *Composites Part A: Applied Science and Manufacturing*, 55(0):188 – 194.

[68] Zhang, W., Suhr, J., and Koratkar, N. A. (2006). Observation of high buckling stability in carbon nanotube polymer composites. *Advanced Materials*, 18(4):452–456.

[69] Zhang, Z., Sun, Z., Yao, J., Kosynkin, D. V., and Tour, J. M. (2009). Transforming carbon nanotube devices into nanoribbon devices. *Journal of the American Chemical Society*, 131(37):13460–13463.